Combustion and Flame 213 (2020) 255–267

Contents lists available at ScienceDirect

Combustion and Flame

journal homepage: www.elsevier.com/locate/combustflame

Kinetics of redox reactions of $CuO@TiO_2–Al_2O_3$ for chemical looping combustion and chemical looping with oxygen uncoupling

Xin Tian, Mingze Su, Haibo Zhao*

State Key Laboratory of Coal Combustion, School of Energy and Power Engineering, Huazhong University of Science and Technology, Wuhan 430074, PR China

ARTICLE INFO

Article history:
Received 29 August 2019
Revised 19 November 2019
Accepted 28 November 2019

Keywords:
Chemical looping
Cu-based oxygen carrier
Redox reaction kinetics
Solid inventory

ABSTRACT

Cu-based materials present as promising oxygen carrier candidates in chemical looping processes, in which CuO can either react directly with fuel gas via heterogeneous gas–solid reaction, or release gaseous O_2 under suitable temperature and O_2 partial pressure, and then react with fuel gas (even solid fuel) via combustion reactions. For comprehensive understandings of the complex reactions of the oxygen carrier in chemical looping processes, as well as for chemical looping reactor design and computational fluid dynamic (CFD) simulation, it is necessary to acquire the reaction kinetics of the oxygen carrier involved therein. This work aims to establish the redox reaction kinetics of a hieratically-structured and high-performance $CuO@TiO_2–Al_2O_3$ oxygen carrier under the context of chemical looping combustion (CLC) and chemical looping with oxygen uncoupling (CLOU). For the investigation, careful efforts have been made to ensure that the kinetics tests were chemical reaction controlled, and theoretical analysis further confirmed negligible effects of gas diffusion in the tests. Well-organized isothermal tests in a thermal gravimetric analyzer (TGA) were then conducted to obtain the solid conversion data needed for reaction kinetics analysis. The oxygen decoupling and subsequent oxygen uptake kinetics of the $CuO@TiO_2–Al_2O_3$ oxygen carrier was first studied. Afterwards, the reactivity of the oxygen carrier with respect to three kinds of fuel gases, *i.e.*, H_2, CO, and CH_4 was evaluated individually. Therefore, kinetics for the relevant reactions of the oxygen carrier in both CLC and CLOU conditions were determined. The conversion of the $CuO@TiO_2–Al_2O_3$ oxygen carrier under different reacting atmosphere was found to subject to different reaction mechanisms. The global activation energies attained for the oxygen decoupling, oxygen uptake, and reduction by H_2, CO, and CH_4 were 217.2 kJ/mol, 87.5 kJ/mol, 44.5 kJ/mol, 40.1 kJ/mol, and 112.2 kJ/mol, respectively. The kinetics parameters were then used to estimate the solid inventory required by the fuel reactor when using the $CuO@TiO_2–Al_2O_3$ as oxygen carrier in both CLC of gaseous fuels and CLOU of coals. For the case of CLC, the minimum solid inventory was 16.0 kg/MW_{th}, 23.6 kg/MW_{th}, and 39.4 kg/MW_{th} when using H_2, CO, and CH_4 as fuel gas, respectively. Moreover, typical low oxygen carrier inventory, *i.e.*, 124.2 kg/MW_{th}, was needed to fully combust a Chinese lignite at 950 °C under CLOU condition. The high redox reactivity of the $CuO@TiO_2–Al_2O_3$ demonstrated the feasibility of using this material as oxygen carrier in chemical looping processes.

1. Introduction

With growing concerns on CO_2 emission and the accompanying global warming threat, extensive efforts have been made worldwide to alleviate CO_2 emissions to the atmosphere [1–3]. Chemical looping combustion (CLC), holding the merit of inherent CO_2 separation, has been identified as a promising option to capture CO_2 at low cost and high efficiency. The chemical looping concept was first proposed by Lewis and Gilliland [4] in a patent in 1954, mainly for the purpose of producing high-purity CO_2 stream. Decades later in the 1980s, Richter and Knoche [5] further put forward the idea of replacing the traditional air combustion process by CLC, aiming to improve the exergy efficiency of the power plant system. And this has been widely accepted as the starting point of the CLC technique. Since then, the research on CLC has witnessed a rapid development worldwide. Central to the CLC technique is the application of suitable oxygen carrier as well as reactor with appropriate configuration to realize the cyclic redox loop involved therein [6]. Up to date, over 1200 different kinds of oxygen carriers have been tested in literatures and dozens of chemical looping combustors with thermal power ranged from kW_{th} to

* Corresponding author.
E-mail address: hzhao@mail.hust.edu.cn (H. Zhao).

https://doi.org/10.1016/j.combustflame.2019.11.044
0010-2180/

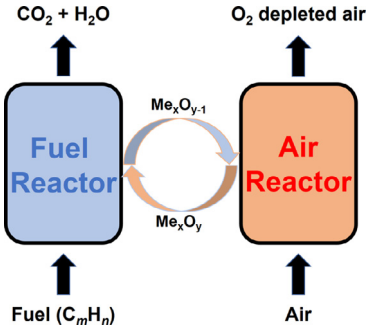

Fig. 1. Schematic of the CLC process.

MW_{th} have been constructed and operated [7–11]. Figure 1 shows a schematic view of the CLC process, in which two sequential reduction–oxidation reactions are repeated in an interconnected fluidized bed reactor system formed by the air reactor (AR) and fuel reactor (FR).

As it is shown in Fig. 1, the fuel in CLC is converted by the lattice oxygen donated from a solid oxygen carrier (Me_xO_y), thus avoids direct contact between fuel and air. To be more specific, in the FR, the fuel is oxidized to generate a highly concentrated CO_2 stream, while the oxygen carrier is reduced due to its oxygen donation, as reaction (1). It should be noted here that, the fuel in reaction (1) is assumed to be in gas phase and it is converted via the gas–solid reaction. Subsequently, the reduced oxygen carrier (Me_xO_{y-1}) recuperates its oxygen capacity in the AR by absorbing O_2 from air, see reaction (2). In this regard, the fuel combustion mode in CLC is totally different from that in traditional air combustion process, and such a change eventually leads to the following advantages: (i) no dilution of combustion products by nitrogen, so as to enable inherent CO_2 capture [6]; (ii) splits the one-step conventional combustion process into two steps, thus realizes cascade utilization of energy [12]; (iii) inhibits prompt NO_x and thermal NO_x formation due to the N_2-free environment in the FR and the relatively low operation temperatures (< 1000 °C) [13].

$$C_mH_n + Me_xO_y \rightarrow (2m+n)Me_xO_{y-1} + mCO_2 + n/2H_2O \quad (1)$$

$$Me_xO_{y-1} + 1/2O_2 \rightarrow Me_xO_y \quad (2)$$

Most of the oxygen carriers proposed in literatures are based on composite materials, using a transition metal oxide as the oxygen donor, and then mixed with an inert support to improve the mechanical performance of the resulted particles [7]. With some kinds of metal oxides, gaseous oxygen can be released under the FR conditions according to the following reaction,

$$Me_xO_y \rightarrow Me_xO_{y-1} + 1/2O_2 \quad (3)$$

O_2 stream will be generated before reaction (3) reaches its equilibrium. Under this circumstance, gaseous O_2 reacts directly with the fuel that presents in the FR according to reaction (4), via the so-called chemical looping with oxygen uncoupling (CLOU) process [14]. The presence of fuel in the FR and its consumption of O_2 further facilitates oxygen release of the oxygen carrier. Alternatively, if fuel is not introduced into the reactor, and H_2O/CO_2 is used as carrier gas, O_2/CO_2 stream (even pure O_2) readily for the oxy-fuel combustion technique can be produced at the outlet of the reduction reactor, known as the chemical looping air separation (CLAS) process. In both cases, the reduced oxygen carrier can regenerate its oxygen capacity by reacting with O_2 in air according to reaction (2) in the oxidation reactor.

$$C_mH_n + (m+n/4)O_2 \rightarrow mCO_2 + n/2H_2O \quad (4)$$

Materials based on copper oxides [15–19], combined oxides [20–25], and some kinds of perovskite oxides [26–30] have been demonstrated to exhibit oxygen uncoupling property under appropriate reaction conditions. Owing to the high oxygen carrying capacity and fast reaction kinetics, Cu-based materials have been considered as one of the most promising oxygen carriers for CLOU [7,19],. The oxygen uncoupling property of Cu-based oxygen carriers is of great importance in CLOU of solid fuels, being critical to reach complete fuel combustion and high CO_2 capture efficiency. Moreover, for the CLOU process with gaseous fuels, both heterogeneous gas–solid reactions and oxygen uncoupling followed by homogeneous oxidation of fuel gas by O_2 are involved during fuel conversion [31]. The competitive relevance of each reaction depends on the fuel gas type, fuel gas concentration, reaction temperature, as well as the reactivity of the oxygen carrier itself [32].

To gain insights into the complex competitive reactions in CLOU process, it is necessary to investigate the kinetics of the redox reactions therein. Also, the redox kinetics parameters of the oxygen carrier are essential to the mathematical modeling as well as reactor design of chemical looping processes. During the past years, most of the kinetics works conducted for oxygen carriers in chemical looping processes was on Fe-based materials, while the studies on Cu-based oxygen carriers are less. García-Labiano et al. [33] investigated the reduction kinetics of CuO/Al_2O_3 (contained 10 wt% of CuO) with CH_4, H_2, and CO under the CLC condition. The kinetics tests were conducted at various temperatures (450–800 °C) and fuel gas concentrations (5–70 vol%) in a thermal gravimetric analyzer (TGA). The reactions were stated to be chemical reaction controlled under these conditions, and the shrinking core model (SCM) for platelike geometry of the reacting surface was adopted for kinetics parameters fitting. Abad et al. [34] further studied the reduction kinetics of the same CuO/Al_2O_3 oxygen carrier with syngas, *i.e.*, H_2 + CO. In comparison to be reduced by H_2 and CO separately, the reduction rate of CuO/Al_2O_3 with syngas was found to be the addition of the individual rates for H_2 and CO. The kinetics parameters attained were then used to calculate the reactor design parameters for a CLC system, including the total solid inventory and solid circulation rate. Chuang et al. [35,36] measured the reduction rate of CuO/Al_2O_3 (with 82.5 wt% CuO) with CO, as well as the oxidation rate of the reduced oxygen carrier (a mixture of Cu and Al_2O_3) by O_2 in a fluidized bed reactor. The reduction of CuO by CO was found mainly controlled by external mass transfer at temperatures higher than 500 °C. Moreover, the reduction temperature significantly affected the reduction mechanism of CuO, which at ~250 °C, CO would react with CuO directly in a one-step process (CuO → Cu); however, at temperatures above ~700 °C, CuO would be reduced by the shrinking core mechanism via two consecutive steps (CuO → Cu_2O, Cu_2O → Cu) [35]. For the oxidation of Cu, complete regeneration to CuO can only be achieved at temperatures higher than 600 °C, under which condition the reaction was controlled by a considerable extent of external mass transfer, and two consecutive oxidation steps were involved (Cu → Cu_2O, Cu_2O → CuO) [36]. Goldstein and Mitchell [37] investigated the kinetics of copper oxides reduction by CO in a pressurized TGA, using pure CuO and Cu_2O as the research medium. Efforts have been made to ensure the reactions in TGA were chemically controlled, *i.e.*, running at temperatures no higher than 500 °C, low CO concentrations (1.6–5 vol%), and using small particle size (75–125 μm for CuO, and < 30 μm for Cu_2O). Finally, the kinetics analysis revealed an overall activation energy of 20 kJ/mol and 25 kJ/mol, respectively, for the reduction of CuO and Cu_2O to Cu. It is worth noting that all these kinetics studies on Cu-based oxygen carriers reviewed above were conducted under the background of CLC, in which the oxygen uncoupling property of CuO was not considered. Table 1 summarizes the main kinetics parameters of Cu-based oxygen carriers attained in literatures under CLC conditions.

Table 1
Relevant kinetics works on Cu-based oxygen carriers in CLC processes.

CuO content (wt%)	Support	Reaction conditions[a]	Kinetics parameters[b]	Ref.
CuO → Cu				
10	Al_2O_3	TGA, T = 450–800 °C	SCM	[33]
		5–70 vol% CH_4	n = 0.4, E_a = 60 kJ/mol	
		5–70 vol% H_2	n = 0.6, E_a = 33 kJ/mol	
		5–70 vol% CO	n = 0.8, E_a = 15 kJ/mol	
82.5	Al_2O_3	b-FBR, T = 250–900 °C	DRM	[35]
		1.1–9.77 vol% CO	n = 1.0, E_a = 52 kJ/mol	
		(CuO→Cu_2O)	n = 1.0, E_a = 28 kJ/mol	
		1.1–9.77 vol% CO		
		(Cu_2O→Cu)		
100	–	p-TGA, T = 200–500 °C	DRM	[37]
		1.6–5 vol% CO (CuO→Cu)	n = 0.7, E_a = 20 kJ/mol	
		1.6–5 vol% CO (Cu_2O→Cu)	n = 0.7, E_a = 25 kJ/mol	
82.5	Al_2O_3	b-FBR, T = 250–900 °C	DRM	[38]
		1.1–9.77 vol% H_2	n = 1.0, E_a = 58 kJ/mol	
		(CuO→Cu_2O)	n = 1.0, E_a = 44 kJ/mol	
		1.1–9.77 vol% H_2 (Cu_2O→Cu)		
60	Al_2O_3	TGA, T = 500–800 °C	SCM	[39]
		20–70 vol% H_2	n = 0.55, E_a = 30 kJ/mol	
		20–70 vol% CO	n = 0.8, E_a = 16 kJ/mol	
14	Al_2O_3	TGA, T = 600–800 °C	SCM	[40]
		5–70 vol% CH_4	n = 0.5, E_a = 106 kJ/mol	
		5–70 vol% CO	n = 0.8, E_a = 11 kJ/mol	
		5–70 vol% H_2	n = 0.5, E_a = 20 kJ/mol	
Cu → CuO				
10	Al_2O_3	TGA, T = 500–800 °C	SCM	[33]
		5–21 vol% O_2	n = 1.0, E_a = 15 kJ/mol	
82.5	Al_2O_3	b-FBR, T = 300–750 °C	DRM	[36]
		1.22–7.5 vol% O_2 (Cu→Cu_2O)	n = 1.0, E_a = 40 kJ/mol	
		1.22–7.5 vol% O_2	n = 1.0, E_a = 60 kJ/mol	
		(Cu_2O→CuO)		

[a] Notes for reaction conditions: TGA = thermal gravimetric analyzer; p-TGA = pressurized thermal gravimetric analyzer; b-FBR = batch fluidized bed reactor.
[b] Notes for kinetics parameters: SCM = shrinking core model; DRM = diffusion reaction model.

For both the oxygen uncoupling of CuO and regeneration of Cu_2O, kinetics driving force (reaction temperature) and thermodynamic driving force (difference between the O_2 concentration in gas phase and the equilibrium O_2 partial pressure of the redox pair) are the two factors that can significantly affect the reaction rates. Thus, separation of these two factors is necessary to correctly predict the reaction rates of the CuO/Cu_2O system in CLOU/CLAS processes. Adánez-Rubio et al. [41] analyzed the relevance of temperature and O_2 partial pressure on the oxygen uncoupling and subsequent regeneration rates of the CuO/$MgAl_2O_4$ (with 60 wt% of CuO) oxygen carrier in CLOU. The nucleation and nuclei growth model was found to well describe the evolution of solid conversion *versus* time. Clayton and co-workers [42,43] investigated the decomposition kinetics of CuO and the following oxidation kinetics of Cu_2O in two sequential studies, using two kinds of Cu-based oxygen carriers, *i.e.*, 50_TiO2_MM (50 wt% of CuO supported on TiO_2 via mechanical mixing) and 45_ZrO2_FG (45 wt% of CuO supported on ZrO_2 by freeze granulation). The kinetics analysis results showed that the activation energy for the CuO decomposition was in the range of 58–67 kJ/mol [42]. For the oxidation of Cu_2O, the average activation energy was given as 165 kJ/mol at temperatures below 700 °C, while it was 71 kJ/mol at temperatures higher than 800 °C [43]. Song et al. [44] conducted oxygen uncoupling and oxidation kinetics studies on the CuO/Cu_2O system under the context of CLAS, using CuO/SiO_2 (with 18 wt% of CuO) as oxygen carrier. The Avrami–Erofeev random nucleation and subsequent growth model and phase boundary reaction model were found to fit well the oxygen uncoupling and oxidation experimental data, respectively. Nevertheless, the activation energy attained for the oxidation process was 3 kJ/mol, which might indicate that the reaction tests were affected by mass transfer to some extent. In a study performed by Wang et al. [45], with 60 wt% of CuO supported on three different inert materials (TiO_2, ZrO_2, and SiO_2) as oxygen carriers, the CuO decomposition process was shown to follow the nucleation and nuclei growth model, and the activation energy was attained in the range of 144.9–155.0 kJ/mol. San Pio et al. [46] reported an activation energy of 249.4 kJ/mol for the oxygen uncoupling of the CuO/SiO_2 (with 70 wt% of CuO) oxygen carrier. For another Cu-based oxygen carrier (with 60 wt% of CuO, 23 wt% of Al_2O_3, and 17 wt% of CaO), Hu et al. [47] attained an activation energy of 59.7 kJ/mol and the corresponding pre-exponential factor of 632 m^3/(mol s) for the decomposition of CuO to Cu_2O. Table 2 gathers the relevant kinetics works conducted on Cu-based oxygen carriers under the context of CLOU/CLAS.

As can be seen from above literatures review, the kinetics parameters attained for Cu-based oxygen carriers in chemical looping processes varied significantly from author to author. Many factors can be reasons for these discrepancies, including CuO loading ratio, inert support type, preparation method, particle size, and testing conditions (experimental facility, temperature, gas flow rates, *etc.*). In order to attain accurate kinetics parameters, it is necessary to minimize the effects of the abovementioned external experimental factors as far as possible. This work aims to determine the redox kinetics of the oxygen uncoupling and subsequent regeneration of a CuO@TiO_2–Al_2O_3 oxygen carrier in CLOU/CLAS, as well as its reduction kinetics with gaseous fuels (H_2, CO, or CH_4) in CLC. The CuO@TiO_2–Al_2O_3 oxygen carrier was prepared by the self-assembly template combustion synthesis (SATCS) method, and the attained particles exhibited a hierarchical structure. The unique framework of this composite material was tailor-made to prevent the formation of copper aluminate spinel ($CuAl_2O_4$) and inhibit the sintering of CuO grains at high temperatures [52]. Previous tests in CLC of gaseous fuels, in CLOU of coal [53], and in CLAS for O_2 production [54] have demonstrated the superior reactivity and thermal stabil-

Table 2
Relevant kinetics works on Cu-based oxygen carriers in CLOU/CLAS processes.

CuO content (wt%)	Support	Facility[a]	T (°C)	Kinetics model[b]	E_a (kJ/mol)	Ref.
$CuO \rightarrow Cu_2O$						
60	$MgAl_2O_4$	TGA	875–1000	NNGM (N = 3/4)	270	[41]
45	ZrO_2	TGA	775–925	First order	58	[42]
50	TiO_2	TGA	800–900	First order	67	[42]
18	SiO_2	TGA	800–900	NNGM (N = 2)	315	[44]
			900–975		176	
60	ZrO_2	TGA	Non-isothermal	NNGM (N = 3)	153	[45]
	TiO_2				155	
	SiO_2				145	
70	SiO_2	TGA	700–900	SCM	249	[46]
60	Al_2O_3–CaO	TGA, b-FBR	850–950	SCM	60	[47]
40	ZrO_2	b-FBR	900–985	First order	281	[48]
100	–	TGA	850–950	First order	327	[49]
60	$CuAl_2O_4$	TGA	Non-isothermal	NNGM (N = 2/3)	344	[50]
$Cu_2O \rightarrow CuO$						
60	$MgAl_2O_4$	TGA	850–1000	L-H	32	[41]
50	TiO_2	TGA	600–700	PBM	172	[43]
			800–950	NNGM (N = 1)	68	
45	ZrO_2	TGA	600–700	PBM	165	[43]
			800–950	NNGM (N = 1)	71	
18	SiO_2	TGA	800–900	SCM (N = 2)	3	[44]
			900–975		−43	
77.5	TiO_2–Al_2O_3	TGA	540–600	Surface reaction	51	[51]
				Ion diffusion	79	

[a] Notes for facility: TGA = thermal gravimetric analyzer; b-FBR = batch fluidized bed reactor.
[b] Notes for kinetics model: NNGM = nucleation and nuclei growth model; SCM = shrinking core model; L–H = Langmuir–Hinshelwood mechanistic model; PBM = Pore blocking model.

Table 3
Chemical and physical characteristics of the CuO@TiO_2–Al_2O_3 oxygen carrier.

XRD phases	CuO, TiO_2, Al_2O_3
Theoretical CuO content (wt%)	77.5
Oxygen carrying capacity (wt%)[a]	7.72
Particle size (μm)	74–100
Porosity	0.29
Apparent density (kg/m^3)	4480
Attrition rate (wt%/h)	6.12
Specific surface area, BET (m^2/g)	1.64
Crushing strength (N)[b]	2.2

[a] Determined by decomposition on TGA in pure N_2 at 900 °C.
[b] Average value of 30 repeated measurements.

ity of this material. In this paper, kinetics tests on the CuO@TiO_2–Al_2O_3 oxygen carrier by varying the reaction temperature, O_2 concentration, fuel gas type and concentration, were conducted in a TGA. Temperature programed reduction (TPR) experiments were conducted to determine the appropriate temperature range prior to formal kinetics testing for the reduction of CuO@TiO_2–Al_2O_3 by fuel gases. Eventually, the solid inventory required in the FR with this oxygen carrier under both CLC and CLOU conditions was calculated based on the attained kinetics parameters, and discussion on using the kinetics parameters for reactor design was also provided.

2. Experimental

2.1. Material

The CuO@TiO_2–Al_2O_3 oxygen carrier used in this work was prepared by the self-assembly template combustion synthesis (SATCS) method, which consisted of 77.5 wt% of CuO, 17.5 wt% of Al_2O_3, and 5 wt% of TiO_2. The particles were calcined at 1050 °C in air for 2 h, and particles in the size range of 74–100 μm were used for kinetics testing. Table 3 summarizes the main chemical and physical properties of the fresh particles attained after calcination. More detailed information on the synthesis of this oxygen carrier can be found elsewhere [52–54].

2.2. Experimental section

The kinetics tests were conducted in a TGA produced by Setaram Instrumentation (SETSYS EVO16). To eliminate the effect of mass transfer on the kinetics tests as far as possible, the appropriate experimental conditions were determined carefully prior to the formal tests, by varying the sample weight in the range of 1–15 mg, particle size between 74–300 μm, and gas flow rate from 80 to 200 mL/min. The results showed that using a sample weight lower than 5 mg and particles smaller than 125 μm was able to avoid the gas diffusion control inside the particles. On the other hand, the solid conversion rate was found to change little when the N_2 flow rate exceeded 150 mL/min. Therefore, gas flow rate of 160 mL/min and around 3 mg of oxygen carrier samples in the diameter range of 74–100 μm were used in the formal kinetics tests, to guarantee the minimum influence of external/internal mass transfer. Moreover, for the reduction tests of the oxygen carrier by H_2, CO, or CH_4, temperature programed reduction (TPR) experiments were conducted first to determine the suitable reaction temperature range for the tests with different reducing gases. For the TPR tests, the samples were heated from room temperature to 900 °C at a ramping rate of 5 °C/min, under the atmosphere of 10 vol% H_2 (or 10 vol% CO, or 10 vol.% CH_4), balanced by N_2.

Table 4 shows the experimental conditions used for the kinetics tests of the CuO@TiO_2–Al_2O_3 oxygen carrier in this work, including the reaction temperatures and reactive gas concentrations. The oxygen uncoupling tests were conducted at five different temperatures (810 °C, 830 °C, 850 °C, 870 °C, and 890 °C) in pure N_2 and three different O_2 concentrations (0, 0.5 vol%, and 1.0 vol%) at 900 °C. With respect to the oxygen uptake process, the reaction temperatures varied from 520 °C to 600 °C, and the O_2 concentrations between 5.2 and 21 vol%. For the reduction tests of CuO@TiO_2–Al_2O_3 by H_2, CO, and CH_4, the temperature ranges were determined as 225–325 °C, 300–400 °C, and 675–775 °C, respectively, according to the TPR results. The investigated reducing gas concentrations for H_2 and CO were both in the range of 5–35 vol%, while a relatively lower gas concentration range was used for CH_4 (5–20 vol%) to avoid noticeable carbon deposition. In order to at-

Table 4
Experimental conditions of the CuO@TiO_2–Al_2O_3 oxygen carrier in TGA.

1) Oxygen decoupling tests	
Temperature (°C)	O_2 concentration in N_2 (vol%)
810, 830, 850, 870, and 890	0
900	0, 0.5, and 1
2) Oxygen uptake tests	
Temperature (°C)	O_2 concentration in N_2 (vol%)
520, 540, 560, 580, and 600	21
600	5.2, 10.5, 14, and 21
3) Reduction with H_2	
Temperature (°C)	H_2 concentration in N_2 (vol%)
225, 250, 275, 300, and 325	10
300	5, 10, 15, 20, 25, 30, and 35
4) Reduction with CO	
Temperature (°C)	CO concentration in N_2 (vol%)
300, 325, 350, 375, and 400	10
350	5, 10, 15, 20, 25, 30, and 35
5) Reduction with CH_4	
Temperature (°C)	CH_4 concentration in N_2 (vol%)
675, 700, 725, 750, and 775	15
700	5, 10, 15, and 20

tain stable and reliable experimental data for the kinetics analysis, each test has been repeated for 5 times, and the results at the 5th cycle were adopted for the analysis.

2.3. Data analysis

The solid conversion of the CuO@TiO_2–Al_2O_3 oxygen carrier during the oxygen uncoupling process, as well as the reduction processes with H_2, CO, or CH_4 can be calculated by the following equation,

$$X_i = \frac{m_{\mathrm{Oxi}} - m}{m_{\mathrm{Oxi}} - m_{\mathrm{Re}}} \times 100\% \tag{5}$$

where X_i represents the solid conversion during process i (i can be the oxygen uncoupling process and the reduction process by H_2, CO, or CH_4, denoted as X_{Dec}, X_{Re,H_2}, $X_{\mathrm{Re,\,CO}}$, and X_{Re,CH_4}, respectively); m_{Oxi} is the mass of samples at the fully oxidation state; m_{Re} is the sample mass at the completely oxygen decoupling (or reduction) state; and m is the instantaneous weight of the samples during reaction.

The conversion of the decomposed oxygen carrier during the oxygen uptake process was calculated as,

$$X_{\mathrm{Oxi}} = \frac{m - m_{\mathrm{Re}}}{m_{\mathrm{Oxi}} - m_{\mathrm{Re}}} \times 100\% \tag{6}$$

The conversion rate of oxygen carrier at different processes can be attained from the derivative of the corresponding solid conversion with respect to time, as,

$$\frac{\mathrm{d}X}{\mathrm{d}t} = \frac{|\mathrm{d}m/\mathrm{d}t|}{m_{\mathrm{Oxi}} - m_{\mathrm{Re}}} \tag{7}$$

3. Results

3.1. Theoretical analysis on the gas diffusion effects in TG tests

Before the acquisition of reaction kinetics parameters, theoretical analysis was conducted to confirm negligible effects of external and internal gas diffusion effects of the redox reactions conducted in this work. Here, the oxygen uptake process of the oxygen carrier was analyzed as an example to illustrate the detailed analysis procedure. To be more representative, the test at the most stringent reaction condition of the oxygen uptake process (600 °C and 21.0 vol% O_2) was chosen for the analysis.

The oxygen carrier samples in TG tests were assumed to be in a static fluid environment, thus the Sherwood number, $Sh = k_g d_p / D_G$, of the particle was considered to be 2 [55]. k_g here is the external mass transfer coefficient, d_p is the diameter of the oxygen carrier particle, and D_G is the molecular diffusivity of the reacting gas in N_2. Therefore, k_g can be calculated as $k_g = 2D_G/d_p$.

The Damkohler number criterion, Da, was adopted to estimate the external gas diffusion effect [56],

$$\mathrm{Da} = r_p R / k_g c_s < 0.15/n|_{n=1} \tag{8}$$

where r_p is the radius of the particle, R is the observed reaction rate per unit particle volume, and it can be obtained from TGA tests, c_s is the reactant concentration at the external surface of the particle, and n is the reaction order.

At 600 °C, the O_2 diffusivity in N_2 is $D_G = 7.69 \times 10^{-5}$ m^2/s, and considering the particle size as $d_p = 100$ μm, thus $k_g = 1.54$ m/s. The O_2 concentration at the external surface of the particle was $c_s = 2.92$ mol/m^3 (21.0 vol% O_2 at 600 °C). Based on the largest oxidation rate attained under the aforementioned reaction condition, $dX_{\mathrm{oxi}}/dt = 0.036$ s^{-1}, the value of R was determined as 438.0 $mol/(m^3\ s)$. Accordingly, the Damkohler number was calculated as $\mathrm{Da} = 4.88 \times 10^{-3}$, far smaller than 0.15. With the same analysis method, the Damkohler number under the other reacting atmosphere was also attained. Table 5 summarizes the key parameters attained for the calculation of the Damkohler number during the O_2 release, O_2 uptake, and the reduction processes with H_2, CO, and CH_4 of the CuO@TiO_2–Al_2O_3 oxygen carrier. As can be concluded, the external gas diffusion resistance was not significant in all tests.

For the effective diffusivity of the reactant within the internal pore of the oxygen carrier, D_e, is approximated as [56],

$$1/D_e = 1/D_{\mathrm{Ke}} + 1/D_{\mathrm{Ge}} \tag{9}$$

where $D_{\mathrm{Ge}} = D_G \theta_p / \tau$ is the effective molecular diffusivity; $D_{\mathrm{Ke}} = 1.94 \times 10^4 \sqrt{T/M}\, \theta_p^{\,2} / \tau S_l \rho_p$ is the effective Knudsen diffusivity; the porosity of the particle, $\theta_p = 0.29$, was determined by the ratio of the apparent density ($\rho_p = 4480$ kg/m^3) to the skeletal density of the particle; the tortuosity, τ, is assumed to be 5.0; $S_l = 1640$ m^2/kg is the surface area; T is the reaction temperature and M is the relative molecular weight of the reactant.

According to the Weise–Prater criterion, to ensure the effectiveness factor higher than 0.95 ($\eta \geq 0.95$) in an isothermal spherical particle, it requires [57],

$$\Phi = R r_p^{\,2} / D_e c_s < 1 \tag{10}$$

For the oxygen uptake process of the oxygen carrier at 600 °C and 21.0 vol% O_2, the value of D_{Ge} and D_{Ke} was attained as $D_{\mathrm{Ge}} = 4.46 \times 10^{-6}$ m^2/s and $D_{\mathrm{Ke}} = 2.32 \times 10^{-4}$ m^2/s, respectively, based on the above equations. Thus, $D_e = 4.38 \times 10^{-6}$ m^2/s, and this led to a Φ value of 8.57×10^{-2}, far smaller than 1. The same analysis procedure was adopted to calculate the Φ value under the other reacting atmosphere. Table 6 gathers the key parameters attained for the calculation of Φ during the O_2 release, O_2 uptake, and the reduction processes with H_2, CO, and CH_4 of the CuO@TiO_2–Al_2O_3 oxygen carrier. As it can be seen, the internal pore diffusion resistance was not significant in all tests either.

3.2. Oxygen decoupling and oxygen uptake kinetics determination

As abovementioned, for the determination of the oxygen decoupling and oxygen uptake kinetics of Cu-based oxygen carrier, the equilibrium O_2 partial pressure (PO_2, eq) of the CuO/Cu_2O system should be both considered when analyzing the thermodynamic driving force. Figure 2 shows the equilibrium O_2 partial pressure of the CuO/Cu_2O redox pair at different temperatures, which were reproduced from the calculation equations shown in previous publications by Adánez-Rubio et al. [41], Clayton and Whitty [42], and Wen et al. [58], see Eqs. (11), (12), and (13), respectively.

Table 5
The key parameters for the calculation of Da under different reacting atmosphere.

	T, K	c_s, mol/m^3	D_G, m^2/s	k_g, m/s	R, mol/(m^3 s)	Da
O_2 release	1173	0.050	7.69×10^{-5}	1.54	78.1	5.08×10^{-2}
O_2 uptake	873	2.92	7.69×10^{-5}	1.54	438.0	4.88×10^{-3}
H_2	573	7.42	1.21×10^{-4}	2.42	767.9	2.14×10^{-3}
CO	623	6.82	4.39×10^{-5}	0.89	1550.1	1.29×10^{-2}
CH_4	1048	1.74	1.11×10^{-4}	2.22	128.8	1.67×10^{-3}

Table 6
The key parameters for the calculation of Φ under different reacting atmosphere.

	T, K	c_s, mol/m^3	D_{Ge}, m^2/s	D_{Ke}, m^2/s	D_e, m^2/s	Φ
O_2 release	1173	0.050	4.46×10^{-5}	2.69×10^{-4}	4.39×10^{-4}	8.90×10^{-1}
O_2 uptake	873	2.92	4.46×10^{-6}	2.32×10^{-4}	4.38×10^{-6}	8.57×10^{-2}
H_2	573	7.42	7.02×10^{-6}	1.88×10^{-4}	6.77×10^{-6}	3.82×10^{-2}
CO	623	6.82	2.55×10^{-6}	1.96×10^{-4}	2.51×10^{-6}	2.26×10^{-1}
CH_4	1048	1.74	6.44×10^{-6}	2.54×10^{-4}	6.28×10^{-6}	2.95×10^{-2}

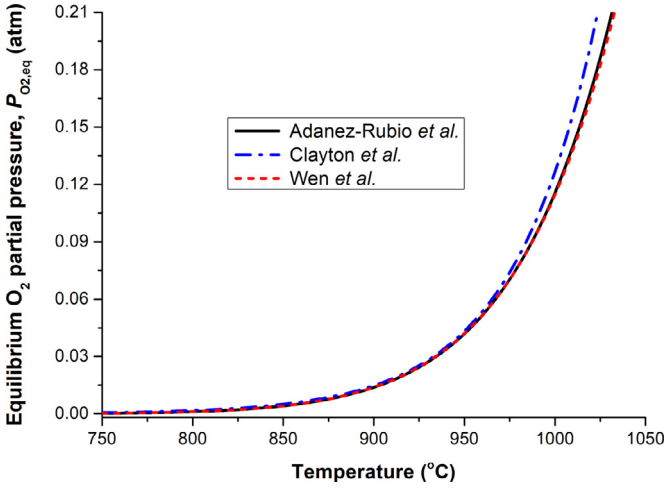

Fig. 2. Calculated equilibrium O_2 partial pressure of the CuO/Cu_2O system at different temperatures. Calculation equations collected from published papers by Adánez-Rubio et al. [41], Clayton and Whitty [42], and Wen et al. [58].

As can be seen, the calculated results based on the three different equations adopted in literatures agreed quite well with each other in the temperature interval of 750–950 °C. However, when the temperature exceeded 975 °C, obvious discrepancy appeared when compared the result of Clayton et al. with those of Adánez-Rubio et al. and Wen et al. As the investigated temperature range for the oxygen decoupling process was 810–900 °C in this work, thus the equilibrium O_2 partial pressure of the CuO/Cu_2O system used later in the kinetics analysis was the average value of the results calculated by the abovementioned three equations. Moreover, considering the fact that the equilibrium O_2 partial pressure of the CuO/Cu_2O system was negligible at temperatures lower than 750 °C, thus it was set to be 0 in the kinetics analysis during the oxygen uptake process (the investigated temperature range was 520–600 °C).

$$P_{O_2,eq(1)} = \exp(22 - 2.993 \cdot 10^4 T^{-1} - 1.048 \cdot 10^6 T^{-2}) \quad (11)$$

$$P_{O_2,eq(2)} = 6.057 \times 10^{-11} e^{0.02146 \times T} \quad (12)$$

$$P_{O_2,eq(3)} = \exp\left[-9.383\left(\frac{1000}{T}\right)^4 + 47.54\left(\frac{1000}{T}\right)^3 - 86.30\left(\frac{1000}{T}\right)^2 + 48.45\left(\frac{1000}{T}\right) - 2.473\right] \quad (13)$$

Figure 3 shows the solid conversion *vs.* time curves of the CuO@TiO_2–Al_2O_3 oxygen carrier during the oxygen decoupling process (CuO → Cu_2O) at five different temperatures in pure N_2 atmosphere (Fig. 3(a)) and at three different O_2 concentrations (PO_2) at 900 °C (Fig. 3(b)). It can be seen from Fig. 3(a) that the oxygen decoupling rate increased obviously along with the increase of temperature in pure N_2 atmosphere. According to the oxygen decoupling rate of Cu-based oxygen carrier given by Eq. (14) [42], the increase of oxygen decoupling rate with temperature can be explained by the increase of both kinetics constant and O_2 driving force ($P_{O_2,eq} - P_{O_2}$). Figure 3(b) presents the solid conversion of the CuO@TiO_2–Al_2O_3 oxygen carrier at 900 °C during the oxygen decoupling process, with O_2 concentrations varied from 0 to 0.01 atm. It can be observed that the increase of O_2 concentration in the gas phase at constant temperature would decrease the oxygen decoupling rate significantly, which at 900 °C (with $P_{O_2,eq} = 0.0148$ atm), the time required for complete oxygen release of the CuO@TiO_2–Al_2O_3 oxygen carrier increased from 4 min at $PO_2 = 0$ to 15 min at $PO_2 = 0.01$ atm. This result was also understandable from the respect of Eq. (14): at constant reaction temperature, both the kinetics constant and PO_2, eq remained unchanged, the increase of P_{O_2} in gas phase lowered the difference between $P_{O_2,eq}$ and P_{O_2}, thus leading to the decrease of the oxygen decoupling rate.

$$\frac{dX_{Dec}}{dt} = A \exp\left(-\frac{E}{RT}\right) f(X)(P_{O_2,eq} - P_{O_2})^n \quad (14)$$

Figure 4 depicts the conversion *vs.* time curves attained in TGA for the oxidation of the decomposed oxygen carrier (Cu_2O → CuO) at different temperatures (520–600 °C, Fig. 4(a)) and different PO_2 values (0.052–0.21 atm, Fig. 4(b)). As it can be observed, for the oxidation process of the decomposed oxygen carrier, the kinetics tests were conducted at much lower temperature range than that of the oxygen decoupling step. The relatively lower temperature range setting adopted here was mainly for the purpose of ensuring that the oxygen uptake tests were chemical reaction controlled. Figure 4(a) shows the oxidation conversion *vs.* time curves of the decomposed oxygen carrier at $PO_2 = 0.21$ atm and various temperatures, where experimental results are presented by symbols and model predictions are indicated by lines. In comparison to Fig. 3(a), it can be seen that the oxygen decoupling process of the CuO@TiO_2–Al_2O_3 oxygen carrier was much slower than the oxidation process of the decomposed samples. The reaction temperature exerted a significant impact on the oxidation rate of the decomposed oxygen carrier. To be more specific, an obvious increasing trend can be observed at increased temperature conditions, which the oxidation rate at 600 °C was about 3 times faster

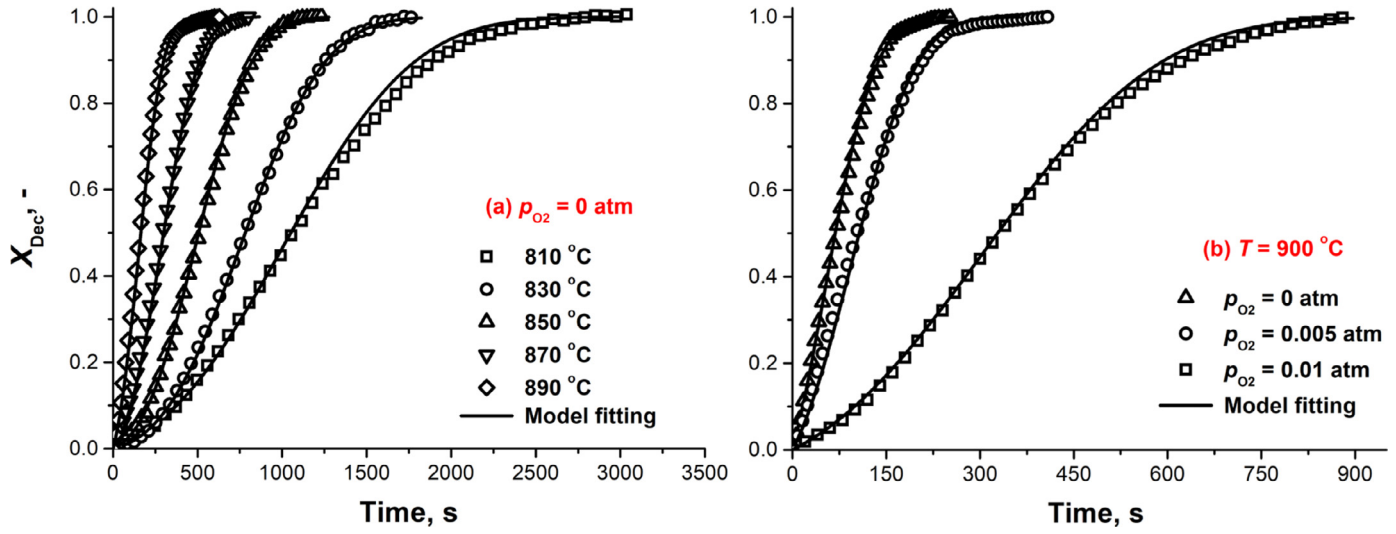

Fig. 3. The solid conversion of the CuO@TiO_2–Al_2O_3 oxygen carrier during the oxygen decoupling process: (a) at different temperatures in pure N_2 atmosphere, and (b) at 900 °C and different O_2 concentrations. Symbols, experimental data; continuous lines, model predictions.

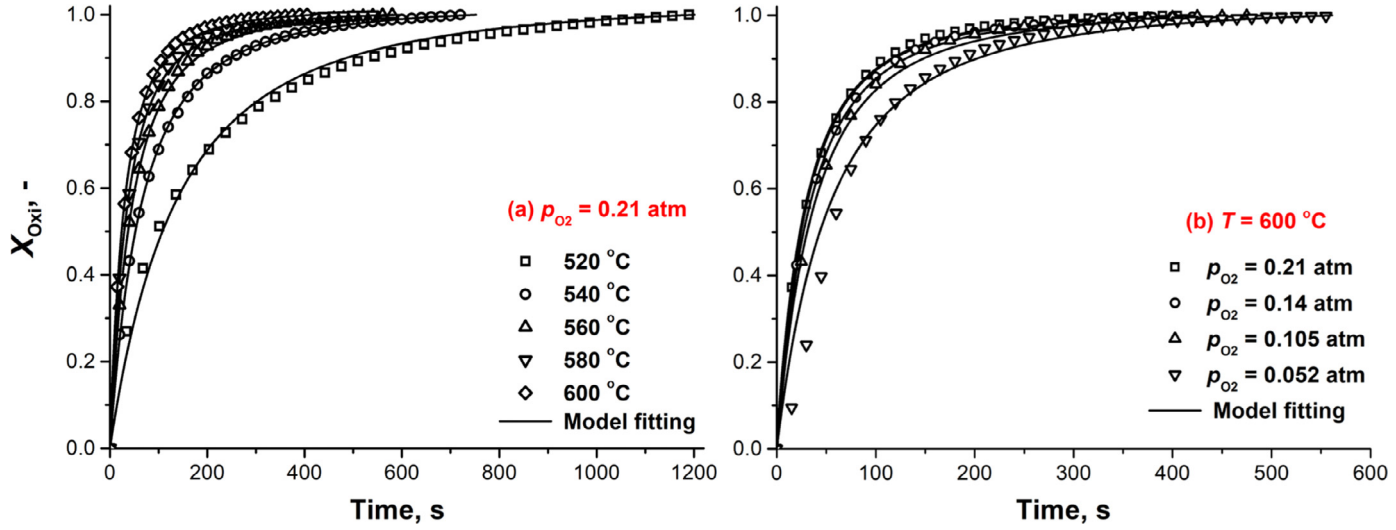

Fig. 4. The solid conversion of the decomposed CuO@TiO_2–Al_2O_3 oxygen carrier during the oxygen uptake process: (a) at different temperatures in a $P_{O_2} = 0.21$ atm, and (b) at 600 °C and different O_2 concentrations. Symbols, experimental data; continuous lines, model predictions.

than that at 520 °C. This result was different from that attained by Adánez-Rubio et al. [41], where the tests were conducted at much higher temperatures (850–1000 °C), and the increase of temperature showed negative effect on the oxidation rate. The difference can be explained by Eq. (14) (the oxygen concentration term in this case will be $(P_{O_2} - P_{O_2,eq})^n$): with the increase of reaction temperature (at constant PO_2), both the kinetics constant and $P_{O_2,eq}$ increased, the increase of kinetics constant improved the oxidation rate, but the increase of PO_2, eq would lower the value of $(P_{O_2} - P_{O_2,eq})^n$ and thus decrease the oxidation rate. Therefore, if the increase of kinetics constant was not able to compensate the decrease of O_2 driving force, lower oxidation rate could be attained at higher temperature condition, like the case studied by Adánez-Rubio et al. [41]. While in this work, the investigated temperatures were much lower, and PO_2, eq always approached to 0, thus the increase of reaction temperature showed negligible impact on the O_2 driving force and an overall enhancing effect on oxidation rate was obtained. Figure 4(b) demonstrates the effect of O_2 concentration in gas phase on the solid conversion of the decomposed oxygen carrier during the oxygen uptake process at 600 °C. The oxidation rate increased with the increase of O_2 concentration in gas phase, being the fastest at $P_{O_2} = 0.21$ atm, due to the increase in the oxygen driving force. When comparing Fig. 4(a) with (b), one can notice that the oxidation process of the decomposed oxygen carrier was mainly controlled by reaction kinetics (temperature), while thermodynamic effect (O_2 concentration in gas phase) was not very significant. This point will be reflected by the reaction order attained in the kinetics reaction rate equation later.

The conversion data obtained under different conditions for the oxygen decoupling and oxygen uptake processes of the CuO@TiO_2–Al_2O_3 oxygen carrier was used for kinetics analysis. The model fitting method was used to select out the most appropriate reaction mechanism. The fitting results indicated that the nucleation and nuclei growth model $(f(X) = 3(1-X)[-\ln(1-X)]^{2/3})$ and chemical reaction model $(f(X) = (1-X)^{3/2})$ can best describe the oxygen decoupling process and oxygen uptake process of the CuO@TiO_2–Al_2O_3 oxygen carrier, respectively. The conversion rate of each test calculated at $X = 0.5$ was then used for linear plot with $\ln(P_{O_2,eq}) - P_{O_2})$ (oxygen decoupling) or $\ln(P_{O_2,eq}) - P_{O_2}$, eq) (oxygen uptake) to obtain the reaction order. As it can be seen

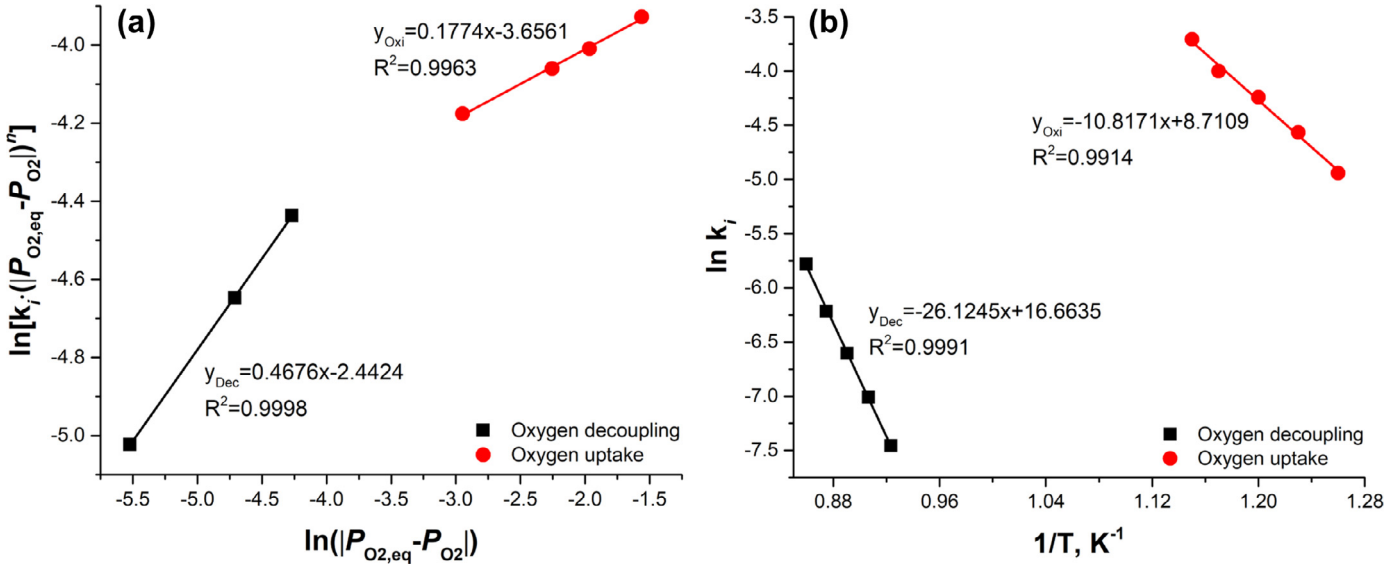

Fig. 5. Arrhenius plots to calculate the kinetics parameters for the oxygen decoupling and oxygen uptake processes of the CuO@TiO_2–Al_2O_3 oxygen carrier: (a) reaction order, and (b) pre-exponential factor and global activation energy.

in Fig. 5(a), the calculated reaction order for the oxygen decoupling and oxygen uptake processes were $n = 0.5$ and $n = 0.2$, respectively.

Once the reaction order was obtained, the kinetics reaction rate constant, k_i, can be calculated according to the following equation,

$$k_i = A\exp\left(-\frac{E}{RT}\right) = \frac{dX_{0.5}}{dt}/\left[f(X_{0.5})(|P_{O_2,eq} - P_{O_2}|)^n\right] \quad (15)$$

where $\frac{dX_{0.5}}{dt}$ is the conversion rate of the oxygen carrier at $X = 0.5$, and $f(X_{0.5})$ is the value of the kinetics function at $X = 0.5$.

With this in mind, the Arrhenius plot with $1000/T$ and $\ln k_i$, *i.e.*, $\ln k_i = -\frac{E}{R}\cdot\frac{1}{T} + \ln A$, at constant P_{O_2} and different temperature conditions (T) was adopted to calculate the activation energy and pre-exponential factor for the oxygen decoupling and oxygen uptake reactions, as shown in Fig. 5(b). The plotting results indicated an activation energy of $E = 217.2$ kJ/mol for the oxygen decoupling process of the CuO@TiO_2–Al_2O_3 oxygen carrier, which is comparable to the value attained by San Pio et al. [46] for an oxygen carrier with 70 wt% CuO supported by SiO_2 (249.4 kJ/mol), and Adánez-Rubio et al. [41] for a material with 60 wt% CuO supported by $MgAl_2O_4$ (245.0 kJ/mol). While for the oxygen uptake process, a much lower activation energy of $E = 87.5$ kJ/mol was attained in comparison to that of the oxygen decoupling process, this result agreed well with the temperature sensitivity of the two reactions as shown in Figs. 3(a) and 4(a). Moreover, the pre-exponential factor for the oxygen decoupling and oxygen uptake processes can also be derived from the Arrhenius plot, as $A = 1.72 \times 10^7\ s^{-1}atm^{-0.5}$ and $A = 8.54 \times 10^3\ s^{-1}atm^{-0.2}$, respectively.

We note here that the oxygen uptake process of the CuO@TiO_2–Al_2O_3 oxygen carrier has been investigated in our previous work from the microscopic mechanism and macroscopic kinetics perspective [51]. Density functional theory (DFT) calculations combined with TGA experimental analysis revealed the activation energy for the two sub-steps of the overall oxygen uptake process, *i.e.*, 50.5 kJ/mol for surface reaction step and 79.2 kJ/mol for the ions diffusion step. The activation energies were attained by a simple mathematical model fitting with unknown parameters of the two sub-steps via global optimization. When comparing the result in ref [51] and that in this work, the global activation energy of $E = 87.5$ kJ/mol for the overall oxygen uptake process of the CuO@TiO_2–Al_2O_3 oxygen carrier attained in this work can be treated as a combining effect of that of the surface reaction step and the ions diffusion step.

Based on the reaction kinetics parameters attained above, the reaction rate equations for the oxygen decoupling and oxygen uptake processes of the CuO@TiO_2–Al_2O_3 oxygen carrier can be expressed as,

$$\frac{dX_{Dec}}{dt} = 5.16\times10^7\exp\left(-\frac{217.2\times10^3}{8.314\cdot T}\right)(1-X)[-\ln(1-X)]^{2/3}(P_{O_2,eq} - P_{O_2})^{0.5} \quad (16)$$

$$\frac{dX_{Oxi}}{dt} = 8.54\times10^3\exp\left(-\frac{87.5\times10^3}{8.314\cdot T}\right)(1-X)^{3/2}(P_{O_2} - P_{O_2,eq})^{0.2} \quad (17)$$

Figure 6 shows the conversion rate *vs.* conversion curves of the CuO@TiO_2–Al_2O_3 oxygen carrier during the oxygen decoupling and oxygen uptake processes, where symbols are results from TGA tests and continuous lines are results calculated by model equations with the attained kinetics parameters. As it can be seen, the maximum oxygen decoupling rate of the oxygen carrier occurred at around $X = 0.5$, while the peak value of the oxidation rate was at the beginning of the oxidation process. The different evolution trend of the oxygen decoupling rate and oxidation rate of the CuO@TiO_2–Al_2O_3 oxygen carrier indicated that the two reactions were indeed subject to different reaction mechanism. Moreover, the peak value of the oxidation rate at 600 °C (in air) was nearly 10 times higher than that of oxygen decoupling rate at 890 °C (in pure N_2), which demonstrated much slower reaction kinetics of the oxygen decoupling process than that of the oxygen uptake process for the CuO@TiO_2–Al_2O_3 oxygen carrier. This result suggested the different appropriate operation temperatures for the FR and AR in CLOU process.

3.3. Reduction kinetics with H_2, CO, or CH_4

As mentioned before, for the reaction of Cu-based oxygen carrier with gaseous fuels, direct gas–solid reaction between oxygen carrier and fuel gas would happen in parallel with the oxygen decoupling reaction of the oxygen carrier (and the following ho-

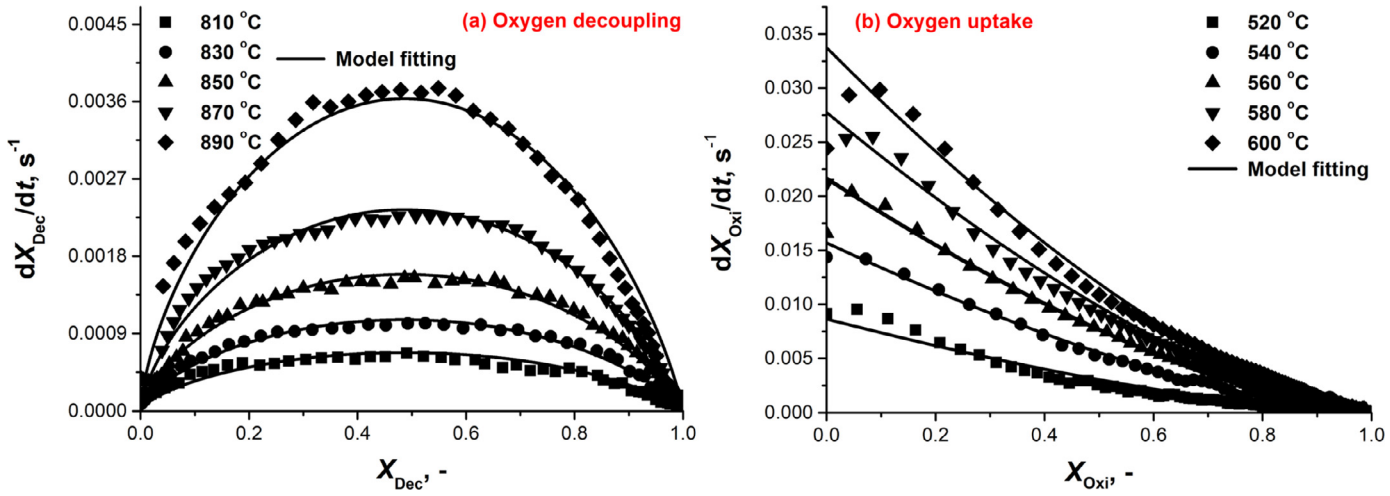

Fig. 6. Conversion rate *vs.* conversion curves of the CuO@TiO_2–Al_2O_3 oxygen carrier at different temperatures: (a) during the oxygen decoupling process in pure N_2, and (b) during the oxygen uptake process in 21 vol% O_2 (N_2 balanced). Symbols, experimental data; continuous lines, model predictions.

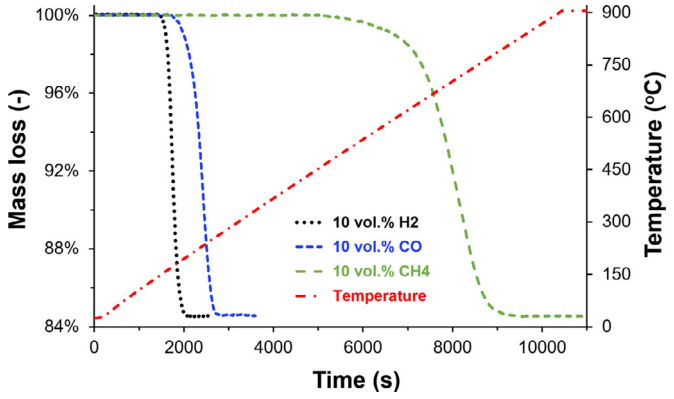

Fig. 7. Normalized mass loss of the CuO@TiO_2–Al_2O_3 oxygen carrier for TPR tests in TGA in 10 vol% H_2, 10 vol% CO, and 10 vol% CH_4, as well as temperature evolution (5 °C/min, with a terminal value of 900 °C).

mogenous reaction between fuel gas and the released O_2). Therefore, to have a comprehensive understanding of the reactions between Cu-based oxygen carrier and gaseous fuels, it is necessary to investigate the reduction kinetics of the oxygen carrier with fuel gases directly, under the context of CLC. Prior to the formal kinetics tests, TPR tests were conducted to determine the most suitable temperature range for the kinetics tests with different reducing gases. In each TPR test, the oxygen carrier samples were first heated to 900 °C (20 °C/min), held there for 30 min, and then cooled down to room temperate. During the whole process, an air stream at 160 mL/min was continuously fed into the reactor, to ensure complete oxidation of the samples. Afterwards, the air stream was switched to the desired reducing gas composition (10 vol% H_2, 10 vol% CO, or 10 vol% CH_4), and the TGA was heated up to 900 °C at a ramping rate of 5 °C/min. The mass loss of the samples during the reaction was automatically recorded by the computer.

Figure 7 shows the normalized mass loss ratio of the samples, $\delta = m/m_{Oxi} \times 100\%$, during the TPR tests in H_2, CO, or CH_4, as well as the temperature evolution profile. As it can be seen, the reaction started at different temperatures for the three fuel gases, being the lowest for H_2 (150 °C), followed by CO (192 °C) and then CH_4 (465 °C). The reduction rates of the oxygen carrier with different fuel gases also varied a lot. In fact, complete solid conversion can be achieved at around 200 °C for the reaction of the CuO@TiO_2–Al_2O_3 oxygen carrier with H_2, while it was 800 °C for the reaction with CH_4. Despite of the varied conversion rates, the normalized mass loss of the oxygen carrier at complete reduction state was the same for the reaction with different fuel gases (*ca.* 15.4 wt%). This result indicated that the total oxygen carrying capacity of the CuO@TiO_2–Al_2O_3 oxygen carrier was the same under different reducing atmosphere. Also, this mass loss ratio was very close to the theoretical oxygen carrying capacity of the CuO@TiO_2–Al_2O_3 oxygen carrier (15.5 wt%, with all CuO content being converted to Cu), which demonstrated the physicochemical stability of the CuO grains in the core-shell framework. According to the TPR results, the reduction of the oxygen carrier with H_2 could occur at very low temperature, while much higher temperature was required for the reaction with CH_4. With these regards, the temperature range selected for the formal reduction kinetics tests was 225–325 °C, 300–400 °C, and 675–775 °C for H_2, CO, and CH_4, respectively.

Figure 8 shows the solid conversion *vs.* time curves of the CuO@TiO_2–Al_2O_3 oxygen carrier with H_2, CO, or CH_4 at different gas concentrations, as well as the linear plot for attaining the reaction order with respect to different fuel gases. As indicated by Fig. 8(a)–(c), the reduction rate of the oxygen carrier was highly related to the fuel gas concentration, which an increase in the fuel gas concentration would accelerate the reduction of the oxygen carrier to certain extents. When looking at the evolution trend of the solid conversion *vs.* time curves, it can be seen that the reaction of the oxygen carrier with CH_4 behaved quite differently in comparison to that with H_2 or CO: Firstly, much higher temperature and longer time were required by CH_4 to achieve complete solid conversion at the same gas concentration than those of H_2 or CO; Secondly, a decrease of the reduction rate with the solid conversion was observed for the reaction with CH_4, while no obvious decrease in reaction rate until the very end of the reaction for that of H_2 or CO. These results indicated that the reaction of CH_4 with the CuO@TiO_2–Al_2O_3 oxygen carrier followed different reaction mechanism with that of H_2 or CO. The model fitting results further confirmed this point, which the reduction process of the oxygen carrier by CO and H_2 can both be well described by the shrinking core model ($G(X) = 1 - (1 - X)^{3/4}$), while the reduction reaction with CH_4 was attributed to the first order nucleation and nuclei growth model ($G(X) = -\ln(1 - X)$). Similar to the linear fitting method used before, the reaction order for the reduction of the CuO@TiO_2–Al_2O_3 oxygen carrier with respect to H_2, CO, and CH_4 was attained as $n = 0.8$, $n = 1.0$, and $n = 0.6$, respectively, as shown in Fig. 8(d). The variation of the reaction order with respect to different fuel gases indicated the different sensitivity of

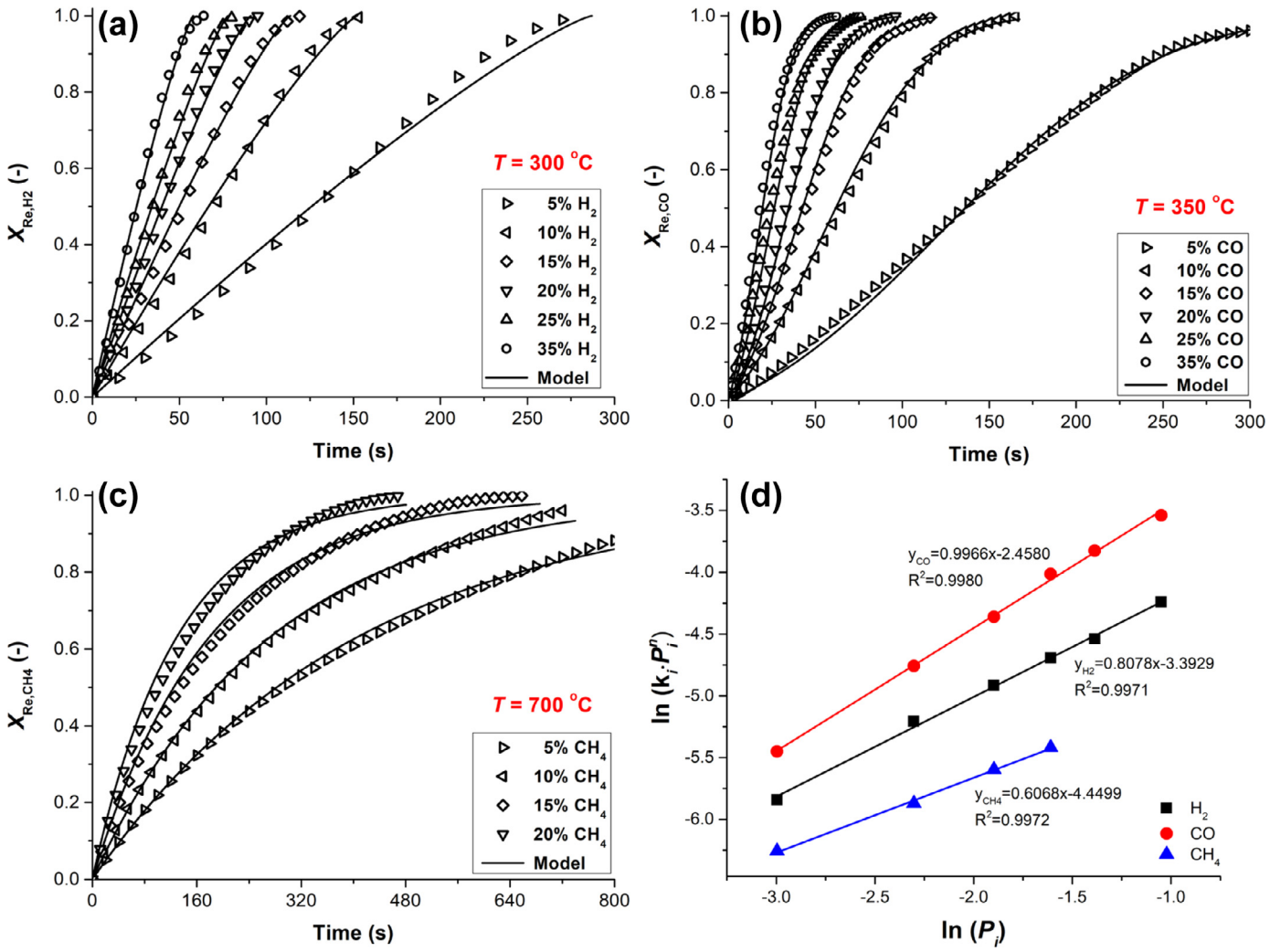

Fig. 8. Effect of gas concentration on the reduction rate of the CuO@TiO_2–Al_2O_3 oxygen carrier with (a) H_2, (b) CO, and (c) CH_4, as well as (d) the plot to obtain the reaction order with respect to H_2, CO, or CH_4. Symbols, experimental data; continuous lines, model predictions (a–c) or fitting results (d).

CuO@TiO_2–Al_2O_3 oxygen carrier to the change of fuel gas concentration.

The effect of temperature on the reduction rate of the oxygen carrier was investigated in different temperature interval for H_2, CO and CH_4. Figure 9(a)–(c) shows the conversion *vs.* time curves for the reduction of the CuO@TiO_2–Al_2O_3 oxygen carrier with 10 vol% H_2, 10 vol% CO, and 15 vol% CH_4 at different temperatures. As it can be seen, the reduction rate of the oxygen carrier was significantly affected by the temperature in all cases, which an increase of temperature would contribute to an obvious increase in the reduction rate. Based on the conversion data of the oxygen carrier with H_2, CO, and CH_4 at different temperatures, together with the kinetics model and reaction order attained above with respect to different fuel gases, the Arrhenius plot with $1000/T$ and $\ln k_i$ at constant fuel gas concentration was adopted again to calculate the activation energy and pre-exponential factor for the reduction reactions with the three kinds of gas fuel, as shown in Fig. 9(d). Finally, the activation energy for the reaction of the CuO@TiO_2–Al_2O_3 oxygen carrier with H_2, CO, and CH_4 was attained as $E =$ 44.5 kJ/mol, $E = 40.1$ kJ/mol, and $E = 112.2$ kJ/mol, and the corresponding pre-exponential factor was $A = 3.50 \times 10^2 \mathrm{atm}^{-0.8}\mathrm{s}^{-1}$, $A = 1.76 \times 10^2 \mathrm{atm}^{-1}\mathrm{s}^{-1}$, and $A = 1.45 \times 10^4 \mathrm{atm}^{-0.6}\mathrm{s}^{-1}$, respectively.

Table 7 compiles the calculated kinetics parameters for chemical reactions of the CuO@TiO_2–Al_2O_3 oxygen carrier investigated in this work, including the oxygen decoupling, oxygen uptake, and the reduction reactions with H_2, CO, and CH_4. The conversion *vs.* time and/or the conversion rate *vs.* conversion curves of these reactions predicted by the reaction model with the obtained kinetics parameters are shown in Figs. 5, 6, 8, and 9. As indicated by these results, the solid conversion of the CuO@TiO_2–Al_2O_3 oxygen carrier under different reacting atmospheres can be well reproduced by the kinetics models in all range of the investigated operating conditions, *i.e.*, different temperature and different gas concentration. We noted here that the operation temperature interval for the realistic CLC/CLOU processes would be much higher. Nevertheless, the intrinsic kinetics reaction data attained in this work at relatively low temperature range is still applicable in the high temperature CLC/CLOU processes, by incorporation of the intrinsic reaction kinetics, the internal and external gas diffusion terms together, as has been illustrated in our previous work [59].

4. Discussion

The obtained kinetics parameters were then used to acquire the design criteria for chemical looping reactors. Based on the method proposed by Abad et al. [31], the minimum solid inventory in the FR when using the CuO@TiO_2–Al_2O_3 as oxygen carrier in CLC of

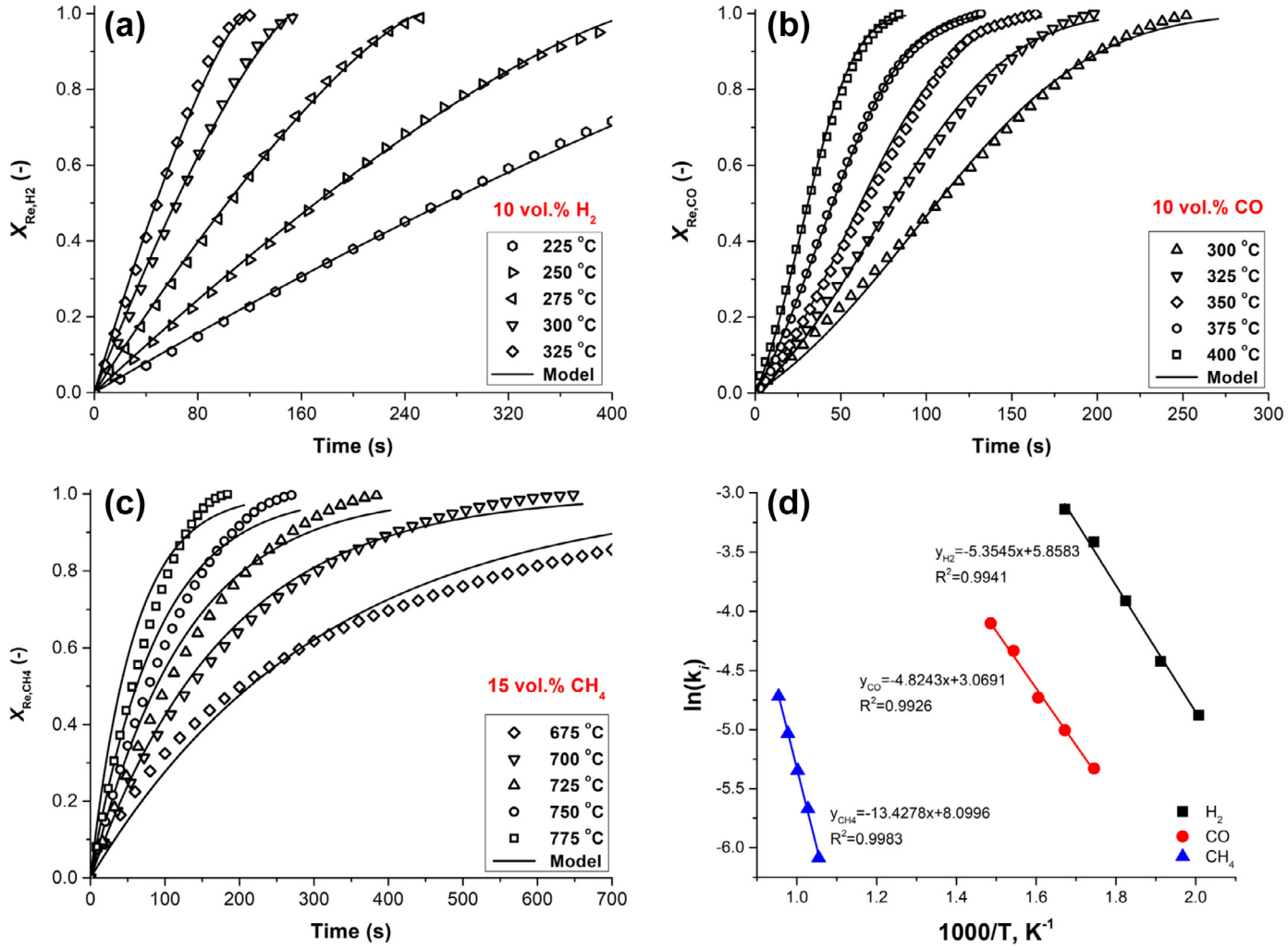

Fig. 9. Effect of temperature on the reduction rate of the CuO@TiO_2–Al_2O_3 oxygen carrier with (a) H_2, (b) CO, and (c) CH_4, as well as (d) the Arrhenius plot for the activation energy and pre-exponential factor for the reaction with H_2, CO, or CH_4. Symbols, experimental data; continuous lines, model predictions (a–c) or fitting results (d).

Table 7
Summary of the kinetics parameters for the oxygen decoupling, oxygen uptake, as well as the reduction reactions with H_2, CO, and CH_4 of the CuO@TiO_2–Al_2O_3 oxygen carrier.

	Kinetics model equation	n (dimensionless)	E (kJ/mol)	A ($atm^{-n}s^{-1}$)
N_2	$G(X) = [-\ln(1-X)]^{1/3}$	0.5	217.2	1.72×10^7
O_2	$G(X) = 2[(1-X)^{-1/2} - 1]$	0.2	87.5	8.54×10^3
H_2	$G(X) = 1-(1-X)^{3/4}$	0.8	44.5	3.50×10^2
CO	$G(X) = 1-(1-X)^{3/4}$	1.0	40.1	1.76×10^2
CH_4	$G(X) = -\ln(1-X)$	0.6	112.2	1.45×10^4

gaseous fuel can be calculated by the following equation,

$$m_{FR,CLC} = \frac{2dM_O}{R_{OC}\Delta H_c^0}\frac{1}{[dX_r/dt]_{X_r\to 0}} \quad (18)$$

while for CLOU of solid fuel, the minimum solid inventory in the FR can be calculated as [41],

$$m_{FR,CLOU} = \frac{10^3 m_O}{R_{OC}\cdot LHV}\frac{1}{[dX_{Dec}/dt]_{max}} \quad (19)$$

where d is the stoichiometry for the complete oxidation between oxygen and fuel gas (mole O per mole of fuel), m_O is the mass of oxygen required per kg of solid fuel to full combustion, M_O is the molar weight of oxygen, R_{OC} is the oxygen carrying capacity of the CuO@TiO_2–Al_2O_3 oxygen carrier (7.7 wt% for CLOU, and 15.5 wt% for CLC), ΔH_c^0 is the standard heat of combustion of the fuel gas ($\Delta H_{c,H_2}^0 = -242$ kJ/mol, $\Delta H_{c,CO}^0 = -283$ kJ/mol, and $\Delta H_{c,CH_4}^0 = -802$ kJ/mol), LHV is the lower heating value of the solid fuel, $[dX_r/dt]_{X_r\to 0}$ is the average reactivity of the oxygen carrier at the characteristic gas fuel concentration and at the solid conversion of $X_r \to 0$, $[dX_{Dec}/dt]_{max}$ represents the maximum oxygen generation rate of the oxygen carrier that can be reached at specified temperature (all the O_2 released can be consumed by the fuel, and the gas phase oxygen concentration was considered to be 0).

Figure 10 shows the calculated minimum solid inventory in the FR when using the CuO@TiO_2–Al_2O_3 oxygen carrier for CLC with gaseous fuels (H_2, CO, and CH_4), and for CLOU with three different rank coals (Shengli lignite (SL), FG bituminous (FG), and Gaoping anthracite (GP)), as well as the O_2 production rate when being applied to CLAS process. For CLC with fuel gases, the calculation was based on the typical operation temperature of 800 °C and the inlet

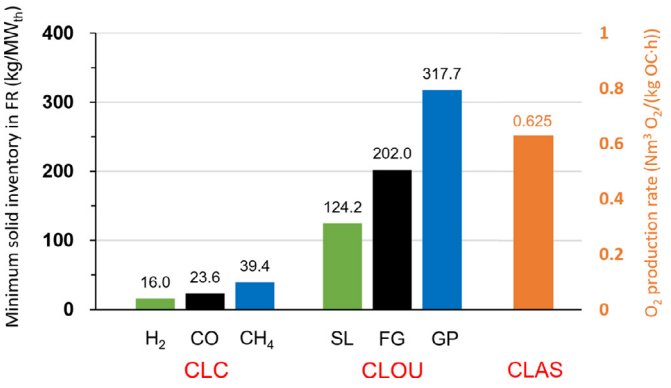

Fig. 10. Minimum solid inventory in the FR for using the CuO@TiO_2–Al_2O_3 oxygen carrier in CLC of gaseous fuels, in CLOU of coals, as well as the O_2 production rate in CLAS process. SL, FG, and GP denote as Shengli lignite, Fugu bituminous, and Gaoping anthracite, respectively.

reactive gas concentration of 50 vol%. For CLOU of solid fuels, the characteristic reaction temperature was selected to be 950 °C, and pure N_2 was used as the carrier gas. Note that, the m_O value for SL, FG, and GP was 1.59, 1.94, and 2.15, and the corresponding *LHV* was 12.82 MJ/kg, 28.85 MJ/kg, and 26.17 MJ/kg, respectively [60]. As it can be seen, very low solid inventory was required when using the CuO@TiO_2–Al_2O_3 as oxygen carrier in CLC of gaseous fuels, as 16.0 kg/MW_{th}, 23.6 kg/MW_{th}, and 39.4 kg/MW_{th} for H_2, CO, and CH_4, respectively. These values were much lower than those reported by García-Labiano et al. [33], in which a kind of CuO/Al_2O_3 material with 10 wt% of CuO (*vs.* 77.5 wt% of CuO in this work) was used as oxygen carrier. The CuO@TiO_2–Al_2O_3 oxygen carrier also showed its superiority when being applied to CLOU of solid fuels. The oxygen carrier inventory in FR was as low as 124.2 kg/MW_{th} when using a typical Chinese lignite (SL) as fuel at 950 °C, lower than the amount of 160 kg/MW_{th} required by the CuO/$MgAl_2O_4$ oxygen carrier (containing 60 wt% of CuO) reported by Adánez-Rubio et al. [41] for another lignite. By the way, when applying this type of oxygen carrier to CLAS process, and considering the average oxygen release rate of 0.0032 s^{-1} at 950 °C, the O_2 production rate would be 0.625 Nm^3 O_2 /(kg OC h).

5. Conclusion

The reduction reactivity of a previously investigated CuO@TiO_2–Al_2O_3 oxygen carrier with core-shell structure was determined in a thermal gravimetric analyzer (TGA) using H_2, CO, or CH_4 as reducing gases. In addition, the oxygen decoupling and oxygen uptake characteristics of this material were investigated by varying the reaction temperature and O_2 concentration in gas phase. These reactions are involved in chemical looping combustion (CLC) and chemical looping with oxygen uncoupling (CLOU) processes. Therefore, redox reaction kinetics of the oxygen carrier under the context of CLC and CLOU were finally established based on the TG data.

Prior to the formal kinetics tests, efforts have been made to eliminate the effects of external and internal gas diffusion on the reactions, and temperature programed reduction (TPR) experiments were conducted to determine the suitable temperature range for the reduction of the oxygen carrier with different fuel gases. The conversion profile of the CuO@TiO_2–Al_2O_3 oxygen carrier was found to be significantly affected by the reacting atmosphere, indicating the different reaction mechanism. TPR results showed different onset temperatures for the reduction of this material by H_2, CO, or CH_4, which demonstrated the varied reactivity of the oxygen carrier towards different fuel gases. To be more specific, the oxygen decoupling and subsequent oxygen uptake processes of the CuO@TiO_2–Al_2O_3 oxygen carrier can be described by the nucleation and nuclei growth model and chemical reaction model, respectively. The corresponding activation energy was attained as 217.2 kJ/mol and 87.5 kJ/mol, and the pre-exponential factor was 1.72×10^7 $atm^{-0.5}s^{-1}$ and 8.54×10^3 $atm^{-0.2}s^{-1}$, respectively. The reduction of the oxygen carrier by H_2 and CO both followed the shrinking core model, with very similar activation energy of 44.5 kJ/mol and 40.1 kJ/mol attained. While the reduction process with CH_4 was subject to the first order nucleation and nuclei growth model, and a higher activation energy of 112.2 kJ/mol was obtained. The kinetics parameters were then used to calculate the minimum solid inventory in the FR when using this oxygen carrier in CLC and CLOU processes. For CLC with H_2, CO, or CH_4 as fuel, the minimum oxygen carrier inventory in FR was calculated as 16.0 kg/MW_{th}, 23.6 kg/MW_{th}, and 39.4 kg/MW_{th}, respectively. While for the CLOU process with a Chinese lignite as fuel, the solid inventory was attained as low as 124.2 kg/MW_{th}. All these results suggested the superior reactivity of the CuO@TiO_2–Al_2O_3 oxygen carrier in chemical looping processes.

Declaration of Competing Interest

The authors declare that they have no known competing financial interests or personal relationships that could have appeared to influence the work reported in this paper.

Acknowledgments

This work was supported by “National Key R&D Program of China (2016YFB0600801)”.

References

[1] T.F. Wall, Combustion processes for carbon capture, Proc. Combust. Inst. 31 (2007) 31–47.
[2] F. Li, L.-.S. Fan, Clean coal conversion processes–progress and challenges, Energy Environ. Sci. 1 (2008) 248–267.
[3] B. Li, Y. Duan, D. Luebke, B. Morreale, Advances in CO_2 capture technology: a patent review, Appl. Energy 102 (2013) 1439–1447.
[4] W. Lewis, E. Gilliland, Production of Pure Carbon Dioxide. U.S. Patent No. 2665971; 1954.
[5] H.J. Richter, K.F. Knoche, Reversibility of combustion process, efficiency and costing, second law analysis of processes, 1983 ACS Symposium Series 235, Washington, DC (1983), pp. 71–85.
[6] A. Lyngfelt, B. Leckner, T. Mattisson, A fluidized-bed combustion process with inherent CO_2 separation; application of chemical-looping combustion, Chem. Eng. Sci. 56 (2001) 3101–3113.
[7] J. Adanez, A. Abad, F. Garcia-Labiano, P. Gayan, F. Luis, Progress in chemical-looping combustion and reforming technologies, Prog. Energy Combust. Sci. 38 (2012) 215–282.
[8] J. Adánez, A. Abad, T. Mendiara, P. Gayán, L. De Diego, F. García-Labiano, Chemical looping combustion of solid fuels, Prog. Energy Combust. Sci. 65 (2018) 6–66.
[9] Q. Imtiaz, D. Hosseini, C.R. Müller, Review of oxygen carriers for chemical looping with oxygen uncoupling (CLOU): thermodynamics, material development, and synthesis, Energy Technol. 1 (2013) 633–647.
[10] T. Song, L. Shen, Review of reactor for chemical looping combustion of solid fuels, Int. J. Greenh. Gas. Con. 76 (2018) 92–110.
[11] H. Zhao, X. Tian, J. Ma, M. Su, B. Wang, D. Mei, Development of tailor-made oxygen carriers and reactors for chemical looping processes at Huazhong University of Science & Technology, Int. J. Greenh. Gas Con. 93 (2020) 102898 http://doi.org/10.1016/j.ijggc.2019.102898.
[12] M. Ishida, J. Hongguang, A new advanced power-generation system using chemical-looping combustion, Energy 19 (1994) 415–422.
[13] M. Ishida, H. Jin, A novel chemical-looping combustor without NO_x formation, Ind. Eng. Chem. Res. 35 (1996) 2469–2472.
[14] T. Mattisson, A. Lyngfelt, H. Leion, Chemical-looping with oxygen uncoupling for combustion of solid fuels, Int. J. Greenh. Gas. Con. 3 (2009) 11–19.
[15] T. Mattisson, H. Leion, A. Lyngfelt, Chemical-looping with oxygen uncoupling using CuO/ZrO_2 with petroleum coke, Fuel 88 (2009) 683–690.
[16] I. Adánez-Rubio, A. Abad, P. Gayán, F. Luis, F. García-Labiano, J. Adánez, Identification of operational regions in the chemical-looping with oxygen uncoupling (CLOU) process with a Cu-based oxygen carrier, Fuel 102 (2012) 634–645.
[17] P. Gayán, I. Adánez-Rubio, A. Abad, F. Luis, F. García-Labiano, J. Adánez, Development of Cu-based oxygen carriers for chemical-looping with oxygen uncoupling (CLOU) process, Fuel 96 (2012) 226–238.

[18] L. Xu, J. Wang, Z. Li, N. Cai, Experimental study of cement-supported CuO oxygen carriers in chemical looping with oxygen uncoupling (CLOU), Energy Fuel 27 (2013) 1522–1530.

[19] T. Mattisson, Materials for chemical-looping with oxygen uncoupling, ISRN Chem. Eng. (2013) Article ID 526375, doi:10.1155/2013/526375.

[20] A. Shulman, E. Cleverstam, T. Mattisson, A. Lyngfelt, Chemical-looping with oxygen uncoupling using Mn/Mg-based oxygen carriers–oxygen release and reactivity with methane, Fuel 90 (2011) 941–950.

[21] G. Azimi, H. Leion, M. Rydén, T. Mattisson, A. Lyngfelt, Investigation of different Mn–Fe oxides as oxygen carrier for chemical-looping with oxygen uncoupling (CLOU), Energy Fuel 27 (2012) 367–377.

[22] V. Frick, M. Rydén, H. Leion, T. Mattisson, A. Lyngfelt, Screening of supported and unsupported Mn–Si oxygen carriers for CLOU (chemical-looping with oxygen uncoupling), Energy 93 (2015) 544–554.

[23] G. Azimi, T. Mattisson, H. Leion, M. Ryden, A. Lyngfelt, Comprehensive study of Mn–Fe–Al oxygen-carriers for chemical-looping with oxygen uncoupling (CLOU), Int. J. Greenh. Gas. Con. 34 (2015) 12–24.

[24] A. Shafiefarhood, A. Stewart, F. Li, Iron-containing mixed-oxide composites as oxygen carriers for chemical looping with oxygen uncoupling (CLOU), Fuel 139 (2015) 1–10.

[25] T. Mattisson, D. Jing, A. Lyngfelt, M. Ryden, Experimental investigation of binary and ternary combined manganese oxides for chemical-looping with oxygen uncoupling (CLOU), Fuel 164 (2016) 228–236.

[26] H. Leion, Y. Larring, E. Bakken, R. Bredesen, T. Mattisson, A. Lyngfelt, Use of $CaMn_{0.875}Ti_{0.125}O_3$ as oxygen carrier in chemical-looping with oxygen uncoupling, Energy Fuel 23 (2009) 5276–5283.

[27] M. Rydén, A. Lyngfelt, T. Mattisson, $CaMn_{0.875}Ti_{0.125}O_3$ as oxygen carrier for chemical-looping combustion with oxygen uncoupling (CLOU)—experiments in a continuously operating fluidized-bed reactor system, Int. J. Greenh. Gas. Con. 5 (2011) 356–366.

[28] N. Galinsky, A. Mishra, J. Zhang, F. Li, CaAMnO (A= Sr and Ba) perovskite based oxygen carriers for chemical looping with oxygen uncoupling (CLOU), Appl. Energy 157 (2015) 358–367.

[29] N. Galinsky, M. Sendi, L. Bowers, F. Li, CaMnBO (B= Al, V, Fe, Co, and Ni) perovskite based oxygen carriers for chemical looping with oxygen uncoupling, Appl. Energy 174 (2016) 80–87.

[30] A. Mishra, T. Li, F. Li, E.E. Santiso, Oxygen vacancy creation energy in Mn-containing perovskites: an effective indicator for chemical looping with oxygen uncoupling, Chem. Mater. 31 (2018) 689–698.

[31] A. Abad, F. García-Labiano, P. Gayán, L. de Diego, J. Adánez, Redox kinetics of $CaMg_{0.1}Ti_{0.125}Mn_{0.775}O_{2.9-\delta}$ for chemical looping combustion (CLC) and chemical looping with oxygen uncoupling (CLOU), Chem. Eng. J. 269 (2015) 67–81.

[32] D. Mei, A. Abad, H. Zhao, J. Adánez, Characterization of a sol–gel derived $CuO/CuAl_2o_4$ oxygen carrier for chemical looping combustion (CLC) of gaseous fuels: relevance of gas–solid and oxygen uncoupling reactions, Fuel Process. Technol. 133 (2015) 210–219.

[33] F. García-Labiano, L.F. de Diego, J. Adánez, A. Abad, P. Gayán, Reduction and oxidation kinetics of a copper-based oxygen carrier prepared by impregnation for chemical-looping combustion, Ind. Eng. Chem. Res. 43 (2004) 8168–8177.

[34] A. Abad, F. García-Labiano, L.F. de Diego, P. Gayán, J. Adánez, Reduction kinetics of Cu-, Ni-, and Fe-based oxygen carriers using syngas ($CO+H_2$) for chemical-looping combustion, Energy Fuel 21 (2007) 1843–1853.

[35] S. Chuang, J. Dennis, A. Hayhurst, S. Scott, Kinetics of the chemical looping oxidation of Co by a co-precipitated mixture of CuO and Al_2O_3, Proc. Combust. Inst. 32 (2009) 2633–2640.

[36] S. Chuang, J. Dennis, A. Hayhurst, S. Scott, Kinetics of the oxidation of a Co–precipitated mixture of Cu and Al_2O_3 by O_2 for chemical-looping combustion, Energy Fuel 24 (2010) 3917–3927.

[37] E.A. Goldstein, R.E. Mitchell, Chemical kinetics of copper oxide reduction with carbon monoxide, Proc. Combust. Inst. 33 (2011) 2803–2810.

[38] S.Y. Chuang, J.S. Dennis, A.N. Hayhurst, S.A. Scott, Kinetics of the chemical looping oxidation of H_2 by a co-precipitated mixture of Cuo and Al_2O_3, Chem. Eng. Res. Des. 89 (2011) 1511–1523.

[39] B. Moghtaderi, H. Song, Reduction properties of physically mixed metallic oxide oxygen carriers in chemical looping combustion, Energy Fuel 24 (2010) 5359–5368.

[40] A. Abad, J. Adánez, F. García-Labiano, F. Luis, P. Gayán, Modeling of the chemical-looping combustion of methane using a Cu-based oxygen-carrier, Combust. Flame 157 (2010) 602–615.

[41] I. Adánez-Rubio, P. Gayán, A. Abad, F. García-Labiano, L.F. de Diego, J. Adánez, Kinetic analysis of a Cu-based oxygen carrier: relevance of temperature and oxygen partial pressure on reduction and oxidation reactions rates in chemical looping with oxygen uncoupling (CLOU), Chem. Eng. J. 256 (2014) 69–84.

[42] C.K. Clayton, K.J. Whitty, Measurement and modeling of decomposition kinetics for copper oxide-based chemical looping with oxygen uncoupling, Appl. Energy 116 (2014) 416–423.

[43] C.K. Clayton, H. Sohn, K.J. Whitty, Oxidation kinetics of Cu_2O in oxygen carriers for chemical looping with oxygen uncoupling, Ind. Eng. Chem. Res. 53 (2014) 2976–2986.

[44] H. Song, K. Shah, E. Doroodchi, T. Wall, B. Moghtaderi, Analysis on chemical reaction kinetics of CuO/SiO_2 oxygen carriers for chemical looping air separation, Energy Fuel 28 (2013) 173–182.

[45] K. Wang, Q. Yu, Q. Qin, Reduction kinetics of cu-based oxygen carriers for chemical looping air separation, Energy Fuel 27 (2013) 5466–5474.

[46] M. San Pio, M. Martini, F. Gallucci, I. Roghair, M. van Sint Annaland, Kinetics of CuO/SiO_2 and CuO/Al_2O_3 oxygen carriers for chemical looping combustion, Chem. Eng. Sci. 175 (2018) 56–71.

[47] W. Hu, F. Donat, S.A. Scott, J.S. Dennis, Kinetics of oxygen uncoupling of a copper based oxygen carrier, Appl. Energy 161 (2016) 92–100.

[48] A.H. Sahir, H.Y. Sohn, H. Leion, J.S. Lighty, Rate analysis of chemical-looping with oxygen uncoupling (CLOU) for solid fuels, Energy Fuel 26 (2012) 4395–4404.

[49] E. Eyring, G. Konya, J. Lighty, A. Sahir, A. Sarofim, K. Whitty, Chemical looping with copper oxide as carrier and coal as fuel, Oil Gas Sci. Technol. – Rev. IFP 66 (2011) 209–221.

[50] L. Guo, H. Zhao, K. Wang, D. Mei, Z. Ma, C. Zheng, Reduction kinetics analysis of sol–gel-derived $CuO/CuAl_2O_4$ oxygen carrier for chemical looping with oxygen uncoupling, J. Therm. Anal. Calorim. 123 (2016) 745–756.

[51] M. Su, J. Cao, X. Tian, Y. Zhang, H. Zhao, Mechanism and kinetics of Cu_2O oxidation in chemical looping with oxygen uncoupling, Proc. Combust. Inst. 37 (2019) 4371–4378.

[52] Z. Xu, H. Zhao, Y. Wei, C. Zheng, Self-assembly template combustion synthesis of a core–shell $CuO@TiO_2–Al_2O_3$ hierarchical structure as an oxygen carrier for the chemical-looping processes, Combust. Flame 162 (2015) 3030–3045.

[53] X. Tian, Y. Wei, H. Zhao, Evaluation of a hierarchically-structured $CuO@TiO_2–Al_2O_3$ oxygen carrier for chemical looping with oxygen uncoupling, Fuel 209 (2017) 402–410.

[54] X. Tian, Y. Wei, H. Zhao, Using a hierarchically-structured $CuO@TiO_2–Al_2O_3$ oxygen carrier for chemical looping air separation in a paralleled fluidized bed reactor, Chem. Eng. J. 334 (2018) 611–618.

[55] M.M. Hossain, H.I. de Lasa, Reactivity and stability of $Co-Ni/Al_2O_3$ oxygen carrier in multicycle CLC, AIChE J. 53 (2007) 1817–1829.

[56] D.E. Mears, Tests for transport limitations in experimental catalytic reactors, Ind. Eng. Chem. Process Des. Dev. 10 (1971) 541–547.

[57] P. Weisz, C. Prater, Interpretation of measurements in experimental catalysis, Adv. Catal. 6 (1954) 143–196.

[58] Y. Wen, Z. Li, L. Xu, N. Cai, Experimental study of natural Cu ore particles as oxygen carriers in chemical looping with oxygen uncoupling (CLOU), Energy Fuel 26 (2012) 3919–3927.

[59] M. Su, H. Zhao, X. Tian, P. Zhang, B. Du, Z. Liu, Intrinsic reduction kinetics investigation on a hematite oxygen carrier by Co in chemical looping combustion, Energy Fuel 31 (2017) 3010–3018.

[60] K. Wang, H. Zhao, X. Tian, Y. Fang, J. Ma, C. Zheng, Chemical-looping with oxygen uncoupling of different coals using copper ore as an oxygen carrier, Energy Fuel 29 (2015) 6625–6635.